Anti-Stokes Raman gain enabled by modulation instability in mid IR waveguides

A. D. Sánchez[1,3,*], P. I. Fierens[2,3], S. M. Hernandez[1], J. Bonetti[1,3], G. Brambilla[4], and D. F. Grosz[1,3]

[1] Grupo de Comunicaciones Ópticas, Instituto Balseiro,Bariloche, Río Negro 8400, Argentina
[2] Grupo de Optoelectrónica, Instituto Tecnológico de Buenos Aires,CABA 1106, Argentina
[3] Consejo Nacional de Investigaciones Científicas y Técnicas (CONICET), Argentina
[4] Optoelectronics Research Centre, University of Southampton SO17 1BJ, England
[*] Corresponding author: alfredo.sanchez@ib.edu.ar

Compiled September 25, 2018

The inclusion of self-steepening in the linear stability analysis of modulation instability (MI) leads to a power cutoff above which the MI gain vanishes. Under these conditions, MI in mid-IR waveguides is shown to give rise to the usual double-sideband spectrum, but with Raman-shaped sidelobes. This results from the energy transfer of a CW laser simultaneously to both Stokes and anti-Stokes bands in pseudo-parametric fashion. As such, the anti-Stokes gain matches completely the Stokes profile over the entire gain bandwidth. This remarkable behavior, not expected from an unexcited medium, is shown not to follow from a conventional four-wave mixing interaction between the pump and the Stokes band. We believe this observation to be of relevance in the area of Raman-based sensors which, in several instances, rely on monitoring small power variations of the anti-Stokes spectral component.

OCIS codes: (190.5650) Raman effect; (190.4380) Nonlinear optics, four-wave mixing

http://dx.doi.org/10.1364/ao.XX.XXXXXX

1. INTRODUCTION

Modulation instability (MI) in waveguides has been thoroughly addressed in the area of fiber optics [1] where it is related to the formation of optical solitons [2], the generation of coherent light in the infrared [3], and the enhancement of four-wave mixing nonlinear interactions in optical communication systems [4], among others.

Complete models of MI in waveguides, see, *e.g.*, [5, 6] and references therein, can be used to analyze the interplay between high-order dispersion, Raman scattering, and self-steepening. This last effect, arising from a first-order expansion of the waveguide nonlinear-coefficient dependence on frequency, is often associated with the break-up of ultrashort pulses upon propagation. However, it also has profound consequences in the case of continuous-wave (CW) pumping of the waveguide, as its inclusion leads to an optimum pump power that maximizes the MI gain [7] and a power cutoff [8] above which the MI gain vanishes, leaving behind only the Raman contribution. Recent work [9] focusing on emerging phenomena beyond this cutoff showed that the remnant gain has a Raman, and frequency-tunable, profile in the Stokes (low-frequency) band. As it is well known, Raman scattering transfers energy from high to low frequencies, a principle used in every Raman discrete and/or distributed amplification scheme [10–12]. As such, the anti-Stokes (high-frequency) component experiences gain only if the transmitting medium provides a population of excited phonons able to transfer energy and create shorter wavelength photons in the anti-Stokes band. This excited phonon population can be achieved, for instance, through thermal excitation, and this is the principle of operation of many distributed Raman temperature sensors which monitor the power of the Stokes and anti-Stokes bands, and whose ratio is highly dependent (through a Bose-Einstein distribution) on the local temperature [13, 14].

In this paper we turn our attention to the behavior of the anti-Stokes band around the MI power cutoff region and find that there is also a Raman-shaped gain beyond the cutoff power. One may suspect that this gain results from the energy transfer, via conventional four-wave mixing, between the pump and the Stokes band. However, we demonstrate that this is not the case and that this process results from a pseudo-parametric interaction, *i.e.*, in the sense that there is no net energy transfer from the CW pump to the transmission medium, where two pump photons are annhilated, and two photons are simultaneously created at the Stokes and anti-Stokes bands, as if in a simple model of modulation instability in waveguides.

The remaining of the paper is organized as follows. In Section 2 we review the numerical model, based on the generalized nonlinear Schrödinger equation, and revisit analytical expressions for a full model of scalar modulation instability in waveguides. In Section 3 we discuss the effect of Raman scattering in both normal and anomalous dispersion regimes, introduce proper metrics to account for the pseudo-parametric nature of the processes involved, underscore the need of including self-steepening in the analysis, and show anti-Stokes gain for the unexcited transmission medium. Concluding remarks are presented in Section 4.

2. FULL MODEL OF MODULATION INSTABILITY

Pulse propagation in a lossless nonlinear waveguide is well described by the generalized nonlinear Schrödinger equation (GNLSE) [15]

$$\frac{\partial A(z,T)}{\partial z} - i\hat{\beta}A(z,T) = i\hat{\gamma}A(z,T)\int_{-\infty}^{\infty} R(T')\left|A(z,T-T')\right|^2 dT', \tag{1}$$

where $A(z,T)$ is the slowly-varying envelope, z is the spatial coordinate, and T is the time coordinate in a comoving frame at the group velocity. $\hat{\beta}$ and $\hat{\gamma}$ are operators related to the dispersion and nonlinearity, respectively, and are defined by

$$\hat{\beta} = \sum_{m\geq 2} \frac{i^m}{m!}\beta_m \frac{\partial^m}{\partial T^m}, \qquad \hat{\gamma} = \sum_{n\geq 0} \frac{i^n}{n!}\gamma_n \frac{\partial^n}{\partial T^n}. \tag{2}$$

β_m are the coefficients of the Taylor expansion of the propagation constant $\beta(\omega)$ around a central frequency ω_0. Similarly, γ_n are the coefficients of the Taylor expansion of the nonlinear parameter. It is usually sufficient to consider the expansion up to the first term. Under this setting, it can be shown that the total number of photons is conserved if $\gamma_1 = \gamma_0/\omega_0$ [16], which is the usual approximation. The function $R(T)$ models the Raman response of the medium. In the next section $R(T)$ is obtained from measurements performed on a chalcogenide waveguide.

A first-order linear perturbation analysis of the GNLSE reveals that, under certain conditions (*viz.*, anomalous dispersion), continuous-wave (CW) solutions are unstable. This phenomenon, known as modulation instability (MI) [1, 3, 17–22], is a parametric process, where two photons from a CW pump are transferred to both low- and high-frequency bands, one photon each. As a result, MI gain is observed in both sides of the pump.

A complete analysis of modulation instability reveals the complex interplay between high-order dispersion, nonlinearity, and Raman scattering (see, *e.g.*, [5, 6]). For the sake of simplicity, let us consider the case where $\beta_m = 0$ for $m > 2$ and $\gamma_n = 0$ for $n > 1$. It can be shown that the MI gain is given by [23]

$$g_{\mathrm{MI}}(\Omega) = 2\max\{-\mathrm{Im}\{K_1(\Omega)\}, -\mathrm{Im}\{K_2(\Omega)\}, 0\}, \tag{3}$$

$$K_{1,2}(\Omega,p) = \frac{p|\beta_2|}{\tau}\Omega(1+\tilde{R}) \pm |\beta_2\Omega|\sqrt{\frac{\Omega^2}{4} - \frac{p\tilde{R}}{\tau^2} + \frac{p^2\tilde{R}^2}{\tau^2}}, \tag{4}$$

where Ω is the deviation from the pump frequency ω_0 and $\tilde{R}(\Omega)$ is the Fourier transform of the Raman response $R(T)$. For convenience, γ_1 and the pump power P_0 have been normalized as $\tau = \gamma_1/\gamma_0$ and $p = P_0/P_{\mathrm{c}}$, where

$$P_{\mathrm{c}} = \frac{|\beta_2|\gamma_0}{\gamma_1^2} \tag{5}$$

is the cutoff power above which the MI gain vanishes, a phenomenon made apparent by the inclusion of γ_1 in the model [7, 8].

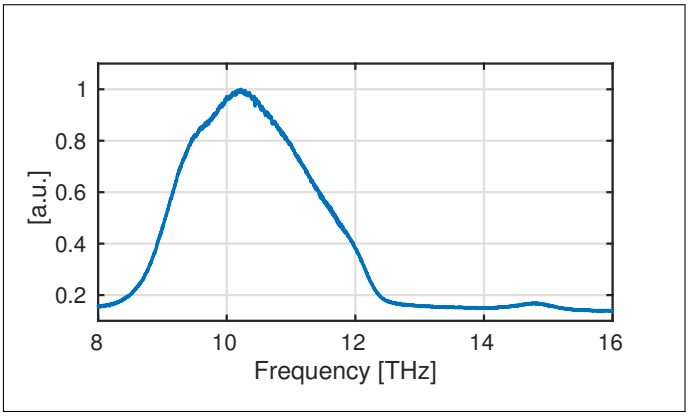

Fig. 1. Measured Raman spectrum of a chalcogenide As_2S_3 optical fiber.

In the absence of Raman scattering ($\tilde{R}(\Omega) = 1$), it is easy to verify that there is no gain when $p > 1$, that is, when the pump power P_0 exceeds P_{c}. However, in the presence of Raman scattering ($\tilde{R}(\Omega) \neq 1$), MI gain exists for $p > 1$. The consequences of this last fact are discussed in the next section.

3. RAMAN AND MODULATION INSTABILITY

Stimulated Raman scattering is a non-parametric process that involves the excitation of molecular vibration modes of the waveguide and, as such, does not conserve the energy of the propagating electromagnetic field. However, it does conserve the number of photons. Qualitatively speaking, the energy exchange experienced by a strong continuous-wave laser involves the annihilation of a pump photon and the simultaneous creation of another photon in the Stokes band. Similarly, a photon in the anti-Stokes band is annihilated and another photon is created at the pump frequency. As a result, gain is observed only in the Stokes band, enabling the application of stimulated Raman scattering in optical amplification [10].

Figure 2 shows simulation results, obtained from an average over 50 noise realizations, of a CW pump co-propagating with additive white Gaussian noise. The signal was propagated an arbitrary distance in the normal dispersion regime of the waveguide. Dispersion and nonlinear parameters are $\beta_2 = 50\ \mathrm{ps}^2/\mathrm{km}$, $\beta_m = 0$ for $m > 2$, $\gamma_0 = 100\ \mathrm{W}^{-1}\mathrm{km}^{-1}$, and the pump frequency is $\omega_0/2\pi = 59.96$ THz. These parameters are consistent with those of a chalcogenide waveguide with low absorption in the mid IR [24–29] (the choice of this particular wavelength range will become clear later on.) Last, the pump power was set to a moderate $P_0 = 50$ W. For the Raman response, we used $R(T) = (1-f_R)\,\delta(T) + f_R h_R(T)$, where f_R weights the contributions of the instantaneous (electronic) and delayed Raman response of the medium [15]. We assumed a typical $f_R = 0.031$ and $\mathrm{Im}\{\tilde{h}_R(\Omega)\}$ was obtained from our measurements of the Raman spectrum, shown in Fig. 1, of a commercial chalcogenide As_2S_3 [30, 31] optical fiber with core diameter of 180 microns. By means of the Kramers–Kronig relations we computed the real part of $\tilde{h}_R(\Omega)$. The inverse Fourier transform of $\tilde{h}_R(\Omega)$ then provides the Raman response function $h_R(T)$ [15, 32]. Note the peak Raman gain at a frequency deviation of 10.74 THz.

Figure 2(a) shows the spectral density at $L_{\mathrm{R}}/2$, as a function of frequency deviations from the central frequency ω_0. L_{R} is defined as the inverse of the peak Raman gain, that is,

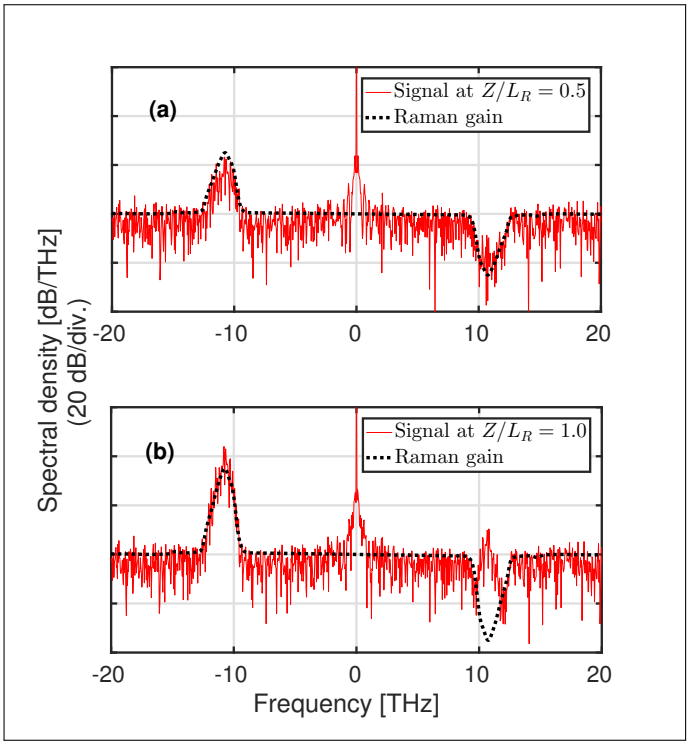

Fig. 2. Simulation results of an average over 50 noise realizations of a CW pump with additive white Gaussian noise: (a) at a propagated a distance $Z = L_R/2$; (b) at $Z = L_R$. The measured Raman gain (black dashed line) is also shown for comparison.

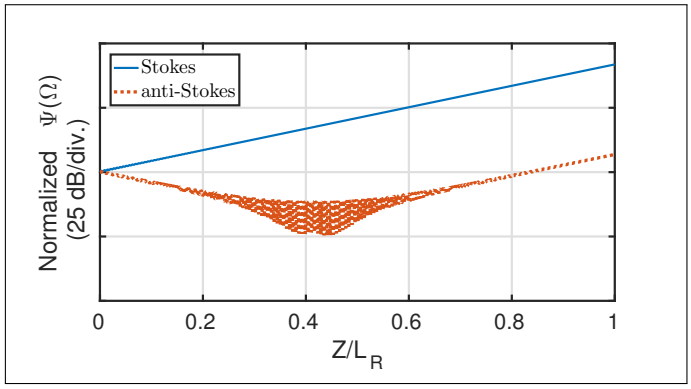

Fig. 3. Results for the normal dispersion regime. Simulation parameters are those of Fig. 2. The Stokes band grows exponentially experiencing Raman gain. The anti-Stokes band is first depleted through Raman power transfer to the pump. Further on into the waveguide, this band experiences gain through FWM.

$L_R = \left[\max\left(-2\mathrm{Im}\left\{\tilde{R}(\Omega)\right\}\right)\right]^{-1}$. We observe that noise in the Stokes band experiences growth through Raman gain. However, in the anti-Stokes band noise decreases as photons are annihilated and new photons are created at the pump frequency. In Fig. 2(b), after the signal propagates the remaining distance, we observe growth in the anti-Stokes band enabled through four-wave mixing (FWM) between the pump and the Stokes component [32].

In order to understand the nature of the processes involved, it is convenient to consider the balance of the number of photons. As it was mentioned, this is a conserved quantity in the presence of Raman scattering. However, when dealing with the large spectral bandwidths associated with Raman processes, the dependence of the nonlinear parameter on frequency, γ_1, must be taken into account. In this scenario, it can be shown that the quantity of photons is conserved if, and only if, $\gamma_1/\gamma_0 = \omega_0^{-1}$ [16]. Note that this implies that the influence of self-steepening increases with decreasing pump frequencies, explaining our choice of the mid-IR spectral range.

Taking these considerations into account, let us define the quantity

$$\Psi(\Omega) = \frac{|A(z,\Omega)|^2}{\hbar\,(\Omega+\omega_0)}, \tag{6}$$

which is proportional to the number of photons at frequency Ω. Here, $A(z,\Omega)$ stands for the Fourier transform of $A(z,T)$. Fig. 3 shows simulation results for the propagation of a pump and two seeds located at the Stokes and anti-Stokes frequencies (∓ 10.74 THz) using the same parameters as in Fig. 2 (both seeds are assumed to have the same number of photons at $z = 0$.) Initially, the number of photons at the anti-Stokes frequency decreases as a consequence of Raman scattering and then begins to increase (at a distance $z \sim 0.4L_R$) due to four-wave mixing between the pump and the Stokes component [33].

Figures 4 shows the evolution of the same quantity in a purely parametric process such as MI in the absence of Raman. The normalized pump power is $p = 0.8$, the fiber dispersion is anomalous, $\beta_2 = -50\ \mathrm{ps}^2/\mathrm{km}$, and γ_0 and ω_0 are those of Fig. 2. The propagated distance is the characteristic MI length, defined as $L_{MI} = (\max\{g_{MI}\})^{-1}$. In Fig. 4(a), $\gamma_1 = 0$ and, given that the number of photons is not conserved, seeds grow unevenly. On the contrary, in Fig. 4(b), $\gamma_1 = \gamma_0/\omega_0$ and both seeds grow evenly. It is evidenced that *proper account of the photon balance in the parametric interaction necessitates the inclusion of self-steepening*.

Now, if the effect of Raman scattering is included, MI gain cannot be the result of a purely parametric process. Recall Fig. 3 where the pump is shown to contribute photons only to the Stokes band, as it is the case with conventional Raman (non-parametric) amplification, and eventually the anti-Stokes band is amplified by means of a FWM interaction between the pump and the Stokes sideband. However, in the anomalous dispersion region of the waveguide, we can have Raman amplification at both low- and high-frequencies simultaneously. Indeed, Fig. 5 shows the evolution of both seeds beyond the cutoff power ($p = 1.1$) and when Raman scattering is factored in. We observe that both seeds grow almost simultaneously (*cf.* Fig. 4(a)), and the slight difference in the growth rate is due to the actual gain of the Stokes band due to Raman. We may regard the resulting behavior as *pseudo-parametric*, intermediate between that of a purely parametric process, such as Fig. 4(b), where the gain evolves simultaneously for low and high frequencies, and that of the Raman (non-parametric) gain in Fig. 3.

Finally, in Fig. 6 the growth of noise clearly shows the amplification of both Stokes and anti-Stokes bands for $p = 3.0$, and up to a propagated distance of $5L_{MI}$. Although not evident from this figure, it can be shown that the gain spectra mimics the shape of the Raman response [9], in both Stokes and anti-Stokes bands.

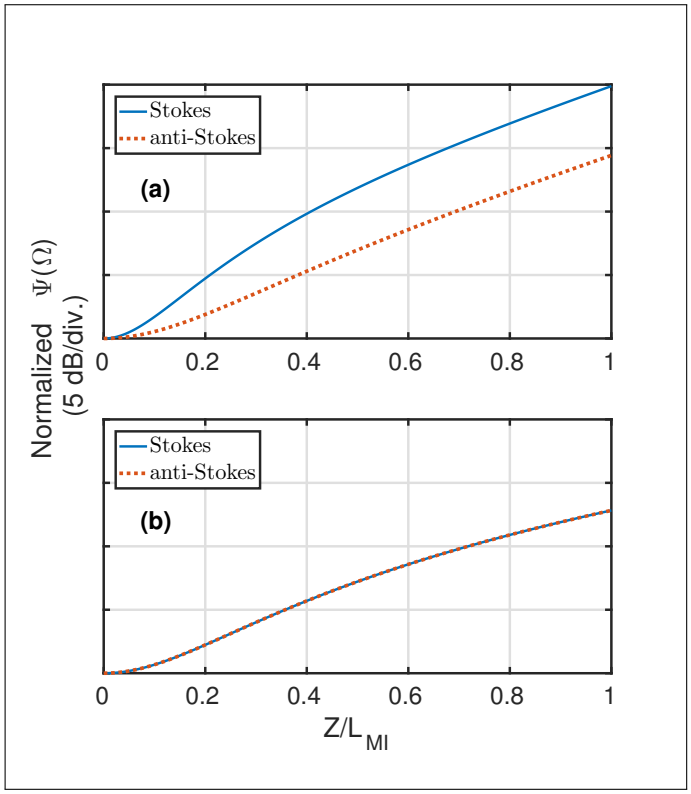

Fig. 4. Anomalous dispersion regime, $p = 0.8$, and no Raman scattering. (a) $\gamma_1 = 0$; (b) $\gamma_1 = \gamma_0/\omega_0$. Note that the inclusion of the self-steepening effect is necessary to ensure the proper photon counting of the parametric interaction.

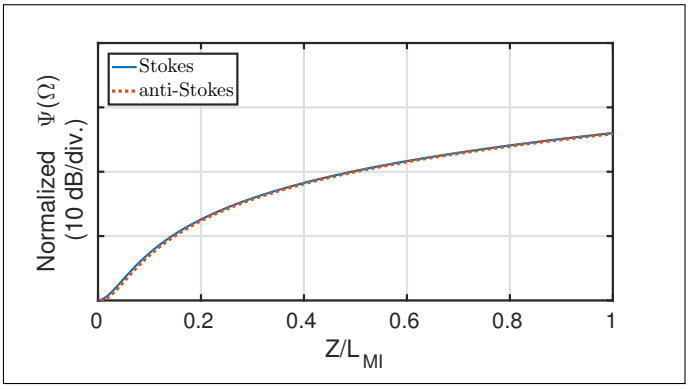

Fig. 5. Anomalous dispersion regime with $p = 1.1$, $\gamma_1 = \gamma_0/\omega_0$ and Raman scattering. Observe the simultaneous growth of both Stokes and anti-Stokes bands, proving that gain in the latter is available right from the start and not as a result of FWM interactions ocurring upon propagation through the waveguide.

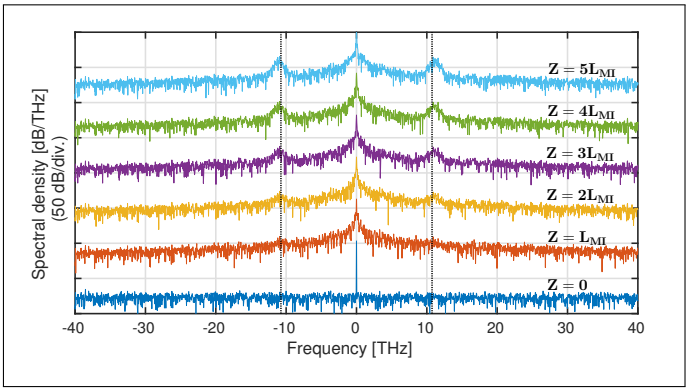

Fig. 6. Noise growth on the Stokes and anti-Stokes bands beyond the cutoff power ($p = 3.0$), and for different propagated distances. Raman peaks at the Stokes and anti-Stokes bands at a measured frequency deviation of ∓ 10.74 THz are also shown (black dotted lines).

4. CONCLUSIONS

In this work we showed that, beyond the cutoff power, modulation instability in mid-IR waveguides gives rise to a double-sideband spectrum, but with Raman-shaped sidelobes. This results from the energy transfer of a CW pump simultaneously to both Stokes and anti-Stokes bands in pseudo-parametric fashion. Furthermore, by explaining the need to include the effect of self-steepening in the model, *i.e.*, the dependence of the waveguide nonlinear parameter in frequency, and introducing proper photon-counting metrics, we demonstrated that the gain in the anti-Stokes band does not result from a four-wave mixing interaction between the pump and the Stokes component and, as such, is readily available from the very beginning of the process. We believe this unexpected behavior in an unexcited transmission medium may find applications, for instance, in the area of Raman-based distributed temperature sensors by providing gain to the anti-Stokes (measured) spectral component, and thus enhancing their sensitivity.

Acknowledgment: We gratefully acknowledge P. Soubelet for measuring the Raman spectrum of the chalcogenide fiber.

REFERENCES

1. K. Tai, A. Hasegawa, and A. Tomita, "Observation of modulational instability in optical fibers," Phys. Rev. Lett. **56**, 135–138 (1986).
2. M. Nakazawa, K. Suzuki, H. Kubota, and H. A. Haus, "High-order solitons and the modulational instability," Phys. Rev. A **39**, 5768–5776 (1989).
3. A. Hasegawa and W. Brinkman, "Tunable coherent IR and FIR sources utilizing modulational instability," IEEE J. Quantum Electron. **16**, 694–697 (1980).
4. D. F. Grosz, C. Mazzali, S. Celaschi, A. Paradisi, and H. Fragnito, "Modulation instability induced resonant four-wave mixing in WDM systems," IEEE Photonics Technol. Lett. **11**, 379–381 (1999).
5. P. Béjot, B. Kibler, E. Hertz, B. Lavorel, and O. Faucher, "General approach to spatiotemporal modulational instability processes," Phys. Rev. A **83**, 013830 (2011).
6. J. Bonetti, S. M. Hernandez, P. I. Fierens, and D. F. Grosz, "Analytical study of coherence in seeded modulation instability," Phys. Rev. A **94**, 033826 (2016).
7. P. K. Shukla and J. J. Rasmussen, "Modulational instability of short pulses in long optical fibers," Opt. Lett. **11**, 171–173 (1986).
8. C. D. Angelis, G. Nalesso, and M. Santagiustina, "Role of nonlinear dispersion in the dynamics of induced modulational instability in kerr media," J. Opt. Soc. Am. B **13**, 848–855 (1996).
9. A. D. Sánchez, S. M. Hernandez, J. Bonetti, P. I. Fierens, and D. F. Grosz, "Tunable raman gain in mid-ir waveguides," J. Opt. Soc. Am. B **35**, 95–99 (2018).
10. M. Ikeda, "Stimulated raman amplification characteristics in long span

single-mode silica fibers," Opt. Commun. **39**, 148 – 152 (1981).
11. D. F. Grosz, A. Agarwal, S. Banerjee, D. Maywar, and A. Kung, "All-raman ultralong-haul single-wideband dwdm transmission systems with oadm capability," J. lightwave technology **22**, 423–432 (2004).
12. M. N. Islam, "Raman amplifiers for telecommunications," IEEE J. selected topics Quantum Electron. **8**, 548–559 (2002).
13. G. Bolognini and A. Hartog, "Raman-based fibre sensors: Trends and applications," Opt. Fiber Technol. **19**, 678 – 688 (2013). Optical Fiber Sensors.
14. M. Wang, H. Wu, M. Tang, Z. Zhao, Y. Dang, C. Zhao, R. Liao, W. Chen, S. Fu, C. Yang, W. Tong, P. P. Shum, and D. Liu, "Few-mode fiber based raman distributed temperature sensing," Opt. Express **25**, 4907–4916 (2017).
15. G. Agrawal, *Nonlinear Fiber Optics*, Optics and Photonics (Academic Press, 2012), 5th ed.
16. K. Blow and D. Wood, "Theoretical description of transient stimulated Raman scattering in optical fibers," IEEE J. Quantum Electron. **25**, 2665–2673 (1989).
17. A. Demircan and U. Bandelow, "Supercontinuum generation by the modulation instability," Opt. Commun. **244**, 181–185 (2005).
18. J. M. Dudley, G. Genty, F. Dias, B. Kibler, and N. Akhmediev, "Modulation instability, Akhmediev breathers and continuous wave supercontinuum generation," Opt. Express **17**, 21497–21508 (2009).
19. D. Solli, C. Ropers, P. Koonath, and B. Jalali, "Optical rogue waves," Nature **450**, 1054–1057 (2007).
20. K. Hammani, C. Finot, B. Kibler, and G. Millot, "Soliton generation and rogue-wave-like behavior through fourth-order scalar modulation instability," Photonics Journal, IEEE **1**, 205–212 (2009).
21. N. Akhmediev, J. M. Soto-Crespo, and A. Ankiewicz, "How to excite a rogue wave," Phys. Rev. A **80**, 043818 (2009).
22. S. T. Sørensen, C. Larsen, U. Møller, P. M. Moselund, C. L. Thomsen, and O. Bang, "Influence of pump power and modulation instability gain spectrum on seeded supercontinuum and rogue wave generation," J. Opt. Soc. Am. B **29**, 2875–2885 (2012).
23. S. M. Hernandez, P. I. Fierens, J. Bonetti, A. D. Sánchez, and D. F. Grosz, "A geometrical view of scalar modulation instability in optical fibers," IEEE Photonics J. **9**, 1–8 (2017).
24. P. Pureza, V. Nguyen, F. Kung, and I. Aggarwal, "Nonlinear properties of chalcogenide glass fibers," J. Optoelectronics Adv. Mater. **8**, 2148–2155 (2006).
25. M. R. Lamont, B. Luther-Davies, D.-Y. Choi, S. Madden, and B. J. Eggleton, "Supercontinuum generation in dispersion engineered highly nonlinear ($\gamma = 10$ /w/m) As_2S_3 chalcogenide planar waveguide," Opt. Express **16**, 14938–14944 (2008).
26. A. Tuniz, G. Brawley, D. Moss, and B. Eggleton, "Two-photon absorption effects on raman gain in single mode As_2Se_3 chalcogenide glass fiber," Opt. express **16**, 18524–18534 (2008).
27. C. Xiong, E. Magi, F. Luan, A. Tuniz, S. Dekker, J. S. Sanghera, L. B. Shaw, I. D. Aggarwal, and B. J. Eggleton, "Characterization of picosecond pulse nonlinear propagation in chalcogenide As_2S_3 fiber," Appl. Opt. **48**, 5467–5474 (2009).
28. B. J. Eggleton, B. Luther-Davies, and K. Richardson, "Chalcogenide photonics," Nat. Photonics **5**, 141–148 (2011).
29. M. R. Karim, B. M. A. Rahman, and G. P. Agrawal, "Mid-infrared supercontinuum generation using dispersion-engineered $Ge_{11.5}As_{24}Se_{64.5}$ chalcogenide channel waveguide," Opt. Express **23**, 6903–6914 (2015).
30. P. Wang, G. Brambilla, M. Ding, X. Zhang, Y. Semenova, Q. Wu, and G. Farrell, "An sms fiber structure based on chalcogenide multimode fiber," in *Nonlinear Optics and Applications VI,* , vol. 8434 (International Society for Optics and Photonics, 2012), p. 84340N.
31. P. Wang, G. S. Murugan, G. Brambilla, M. Ding, Y. Semenova, Q. Wu, and G. Farrell, "Chalcogenide microsphere fabricated from fiber tapers using contact with a high-temperature ceramic surface," IEEE Photon. Technol. Lett **24**, 1103–1105 (2012).
32. R. W. Boyd, *Nonlinear Optics* (Academic Press, 2008).
33. S. Coen, D. A. Wardle, and J. D. Harvey, "Observation of non-phase-matched parametric amplification in resonant nonlinear optics," Phys. review letters **89**, 273901 (2002).